Quantum Electronics **50** (6) 543–550 (2020)

https://doi.org/10.1070/QEL17336

Trapping and detection of single rubidium atoms in an optical dipole trap using a long-focus objective lens

I.I. Beterov, E.A. Yakshina, D.B. Tretyakov, V.M. Entin, U. Singh, Ya.V. Kudlaev, K.Yu. Mityanin, K.A. Panov, N.V. Al'yanova, I.I. Ryabtsev

Abstract. **The trapping of single atoms in optical dipole traps is widely used in experiments on the implementation of quantum processors based on neutral atoms, and studying interatomic interactions. Typically, such experiments employ lenses with a large numerical aperture (NA > 0.5), highly sensitive EMCCD cameras, or photon counters. In this work, we demonstrate trapping and detection of single rubidium atoms using a long-focus objective lens with a numerical aperture NA = 0.172 and a FLir Tau CNV sCMOS camera.**

Keywords: *single atoms, dipole traps, quantum computing.*

1. Introduction

In recent years, a number of experiments have been performed on trapping single alkali metal atoms into optical dipole traps [1–11] and arrays of optical dipole traps [12–20]. Arrays of large dimensions [12–19] and the possibility of arbitrary relocation of atoms to ensure uniform filling of an array [14–16] and the formation of arbitrary spatial configurations of the array of atoms [14, 15, 20] were demonstrated. Prototypes of quantum registers were implemented based on one-dimensional and two-dimensional arrays of single atoms [18, 19].

To trap atoms into optical dipole traps and then detect them by the method of resonance fluorescence, lenses with a large numerical aperture (NA > 0.5) are commonly used [1–21]. This is due to the possibility of using such lenses to focus the laser beam into a spot of small radius (~1 μm) [1, 2], which ensures localisation of trapped atoms and provides conditions for collision blockade [2], when loading of more than one atom into a dipole trap becomes impossible. In addition, the use of lenses with a large numerical aperture increases the efficiency of collecting scattered photons when detecting atoms by the resonance fluorescence method [21].

In experiments on trapping single atoms, short-focus aspherical lenses installed inside a vacuum chamber [1, 2, 4, 9, 12–16] or specially designed multi-lens objectives [7, 8, 17, 18] placed outside a glass cell in front of the vacuum chamber window are widely used. The optical design of such multi-lens objectives compensates for aberrations resulting from the passage of a converging light beam through the vacuum chamber's or the glass cell's window.

Despite the obvious advantages of optical schemes that employ lenses or objective lenses with a large numerical aperture, their principal feature is the placement of optical surfaces at a relatively short distance from a cloud of cold atoms. For lenses placed inside a vacuum chamber, this distance usually does not exceed 5–10 mm [1, 2, 4, 9, 12–16], which leads to the potential occurrence of spurious electric fields in depositing alkali metal atoms on dielectric surfaces. The electronic structure of an atom changes when the latter is deposited on the surface, and the energy levels are hybridised. This is equivalent to the fact that part of the charge is transferred to the substrate on which the atom is located [22]. The uncontrolled electric fields arising in this case significantly complicate experiments with Rydberg states, which are necessary for the implementation of quantum calculations using neutral atoms [23].

Installing an objective lens outside the vacuum chamber, with a typical working distance of 30–60 mm [7, 8, 17, 18], also results in significant restrictions on the size of the vacuum chamber or cell and the amount of internal space used, in particular, when placing electrodes for precision control of electric fields inside the vacuum chamber.

In this regard, it is of interest to use longer-focus objective lenses for conducting experiments with single atoms. The trapping of atoms into an optical dipole trap using a long-focus objective lens with a working distance of 119 mm and NA = 0.172 was described in [8]. At the same time, in this work, a shorter-focus lens with a working distance of 65 mm and NA = 0.291 was used to record the image of trapped atoms. The trapping of atoms was recorded by a photon counter. High quantum efficiency (over 90%) of photon counters is preferable for experiments that employ lenses with a relatively small numerical aperture. However, photon counters do not allow the attainment of a spatial resolution required for the formation and study of arrays of single atoms, which is important in the design of a scalable quantum register.

I.I. Beterov Rzhanov Institute of Semiconductor Physics, Siberian Branch, Russian Academy of Sciences, prosp. Akad. Lavrent'eva 13, 630090 Novosibirsk, Russia; Novosibirsk State University, ul. Pirogova 2, 630090 Novosibirsk, Russia; Novosibirsk State Technical University, prosp. K. Marksa 20, 630092 Novosibirsk, Russia; e-mail: beterov@isp.nsc.ru;
E.A. Yakshina, D.B. Tretyakov, V.M. Entin, K.Yu. Mityanin, N.V. Al'yanova, I.I. Ryabtsev Rzhanov Institute of Semiconductor Physics, Siberian Branch, Russian Academy of Sciences, prosp. Akad. Lavrent'eva 13, 630090 Novosibirsk, Russia; Novosibirsk State University, ul. Pirogova 2, 630090 Novosibirsk, Russia;
U. Singh, Ya.V. Kudlaev Novosibirsk State University, ul. Pirogova 2, 630090 Novosibirsk, Russia;
K.A. Panov Novosibirsk State Technical University, prosp. K. Marksa 20, 630092 Novosibirsk, Russia

Received 11 March 2020, revision received 2 April 2020
Kvantovaya Elektronika **50** (6) 543–550 (2020)
Translated by M.A. Monastyrskiy

In work [9], we successfully demonstrated the possibility of detecting single atoms using a sCMOS camera being inferior in characteristics to EMCCD cameras that are commonly used to observe atoms in arrays of optical dipole traps. At the same time, lenses with a large numerical aperture (NA = 0.5) were used in this work to collect scattered photons of spontaneous fluorescence.

For the EMCCD camera, due to electron multiplication, the read-out noise does not exceed a single electron [9], whereas in the FLir Tau CNV sCMOS video camera, which we used in our experiments, it is two electrons, while in cooled CCD cameras it exceeds six electrons [9]. This significantly degrades the signal-to-noise ratio in recording weak signals. In addition, the quantum efficiency of the FLir Tau CNV camera at a wavelength of 780 nm is ~35%, while for modern Andor Ixon 897 Ultra EMCCD cameras, the quantum efficiency for this wavelength is ~70% [24].

The sensor of the camera we used has a resolution of 1024×960 pixels with a pixel size of 6.5 μm. For comparison, the resolution of the Andor Ixon 897 EMCCD camera is 512×512 pixels at a pixel size of 16 μm, while the more advanced and expensive Andor Ixon 888 EMCCD camera has a resolution of 1024×1024 pixels at a pixel size of 13 μm [24]. The equivalent noise illumination intensity of the FLir Tau CNV camera is 3×10^8 photon cm^{-2}, whereas typical values for EMCCD cameras are 1×10^8 photon cm^{-2} with a measurement time of 33 ms [25].

In this regard, the detection of single atoms using objective lenses with a relatively small numerical aperture and sCMOS cameras is quite difficult. This work demonstrates the trapping and detection of single rubidium atoms with the simultaneous use of a long-focus objective lens with NA = 0.172 for trapping atoms into an optical dipole trap and collecting fluorescence photons in detecting single atoms by means of an sCMOS camera with a short exposure time (50–300 ms).

2. Experimental setup

We used a long-focus TRAP objective lens with a working distance of 119 mm and NA = 0.172, described in [8]. The scheme of the experimental setup is shown in Fig. 1. Radiation of a dipole trap laser (continuous-wave single-frequency Ti:sapphire laser with a ring cavity, wavelength 820 nm) is passed through an acousto-optic modulator, fed into a single-mode polarisation-stable optical fibre and then collimated at its output by a triplet collimator to produce a beam with a diameter of 3 mm. After that, it is reflected from the dichroic mirror and focused by the telescope and objective lens into a cloud of cold rubidium atoms in a magneto-optical trap inside a vacuum chamber.

The Gaussian beam radius is

$$w_0 = \frac{2\lambda f}{\pi d}. \tag{1}$$

Here λ is the radiation wavelength; f is the objective lens's focal length; and d is the Gaussian beam diameter in the aperture. To increase the diameter of the beam incident on the objective lens, a six-fold two-lens telescope is installed in the optical scheme. Thus, the estimated radius of the focused laser beam constitutes 3.5 μm.

The same objective lens is used to collect photons in detecting single atoms by the method of resonance fluorescence. Spontaneous radiation with a wavelength of 780 nm, induced by the cooling lasers of the magneto-optical trap, passes through a dichroic mirror and interference filters that cut off the dipole trap's laser radiation reflected from the telescope lenses, objective lens, and vacuum chamber windows. Then spontaneous radiation is focused onto the FLir Tau CNV sCMOS video camera matrix using an aspherical lens with a focal length of 25 mm. The image recorded by the video camera via the CameraLink interface is saved as a digital array.

To control the spot size of the focused laser radiation of the dipole trap, we used a laser beam spatial distribution meter with scanning slits. The measured two-dimensional intensity profile is shown in Fig. 2a, and the beam cross section along the x axis is shown in Fig. 2b. Approximating the measured profile by the Gaussian distribution gives a waist radius of 4.5 μm, which is somewhat inferior to the calculated value. In addition, certain deviations from the Gaussian profile at the edges of the measured distribution are observed, associated with the optical system aberrations.

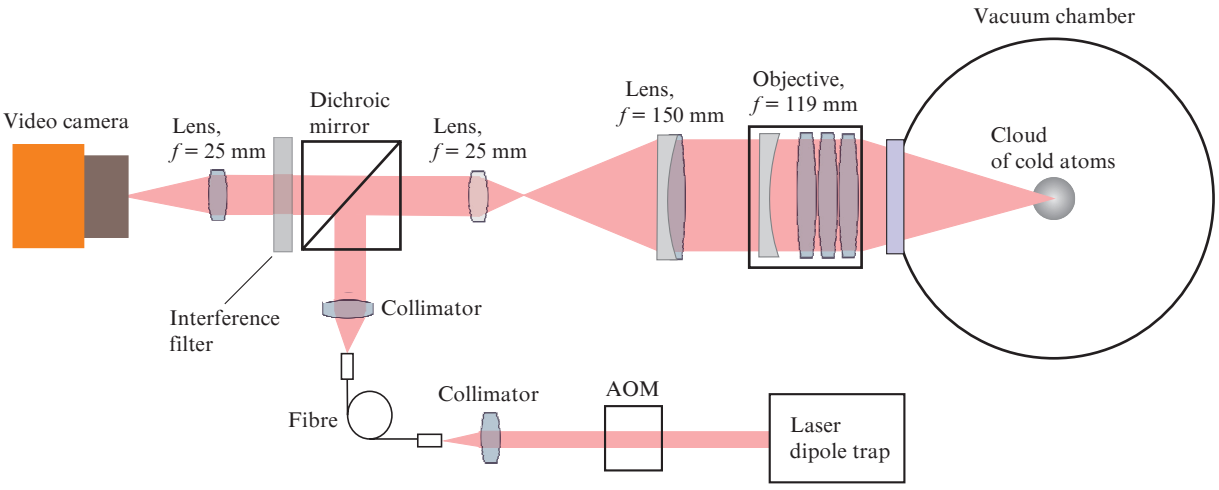

Figure 1. Schematic of the experimental setup for trapping and detecting single rubidium atoms in an optical dipole trap.

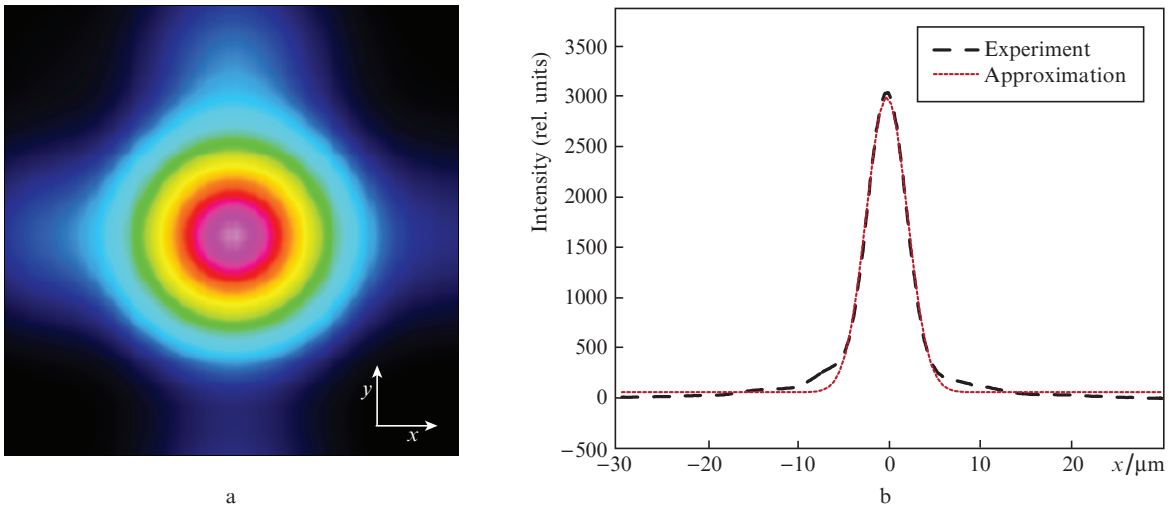

Figure 2. (a) Reconstructed intensity distribution of a focused laser beam with a wavelength of 820 nm and (b) the intensity distribution profile of a focused laser beam along the x axis.

The optical potential depth in a dipole trap for alkali metal atoms and linearly polarised radiation can be estimated as follows [21]:

$$U(r) = \frac{\pi c^2 \Gamma}{2\omega_0^3}\left(\frac{2}{\Delta_2} + \frac{1}{\Delta_1}\right) I(r). \qquad (2)$$

Here, $I(r)$ is the laser radiation intensity at the waist as a function of the distance r from the beam axis; ω_0 is the average transition frequency for the D line; Δ_1 and Δ_2 are the frequency detunings of the dipole trap's laser radiation from the resonance for D_1 and D_2 lines; Γ is the natural width of the D line; and c is the speed of light. The optical potential depth for rubidium atoms, calculated by formula (2) at the trap centre using the Gaussian radiation beam with a wavelength of 820 nm and a waist radius of 4.5 μm at a power of 200 mW, is 6 mK, which is sufficient for trapping atoms into the dipole trap in standard experimental conditions [21].

3. Detection of single atoms in optical dipole trap

To calibrate the system for transferring images of trapped atoms, laser radiation with a wavelength of 820 nm, focused by an objective lens, was fed into a single-mode optical fibre. Then, laser radiation with a wavelength of 780 nm was introduced from the opposite optical fibre's end. Thus, the glowing end-face of the optical fibre turned out located exactly at the place where the atoms should be trapped into the optical dipole trap. An image of the optical fibre's face-end, recorded by a digital video camera, is shown in Fig. 3a. Focusing the radiation into a single pixel of the video camera is desirable to attain the highest possible signal-to-noise ratio when detecting single atoms. At the same time, low optical system magnification caused by the finiteness of the camera pixel's size degrades the spatial resolution, which is undesirable when conducting experiments with arrays of dipole traps.

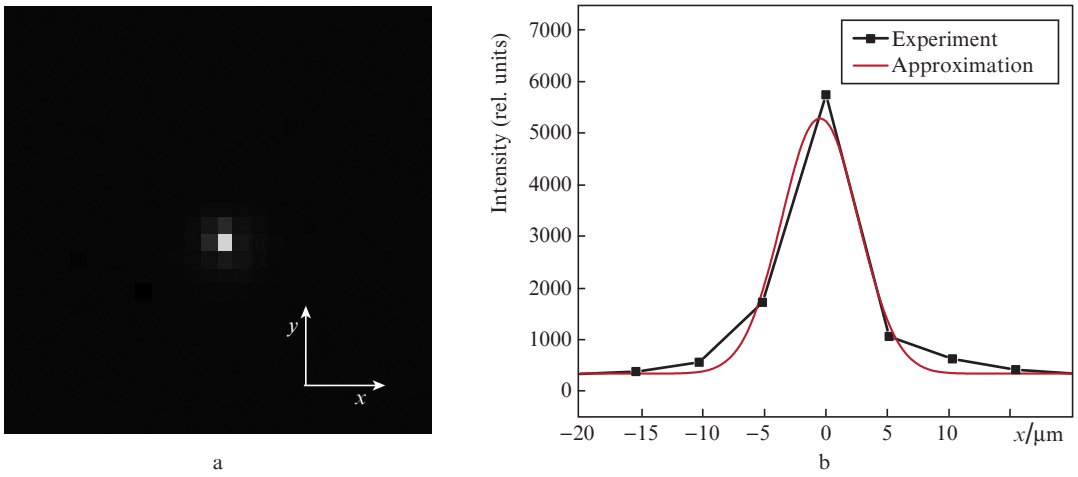

Figure 3. (a) Image of the end-face of a single-mode fibre, placed at the objective lens focus and (b) intensity distribution profile along the x axis for this image, along with its approximation by the Gaussian function.

The intensity distribution profile of the resulting image along the x axis is shown in Fig. 3b. For spatial calibration of the image, a GOST 15114-78 line test pattern was installed at the objective lens focus. Using the pattern image, it was determined that the effective pixel size of the video camera in the object space is 5.15 μm. The measured image radius at the waist, when approximated by a Gaussian profile, was 5.6 ± 0.1 μm. Since the average mode field diameter (MFD) for the fibre we use is 5.3 ± 0.1 μm, we can estimate the standard deviation for the point spread function (PSF) as $\sigma = 2.5 \pm 0.2$ μm, which is generally consistent with the TRAP objective lens data: $\sigma = 1.8 \pm 0.2$ μm [8]. Certain deterioration of the point spread function is due to the optical system's aberrations, which consists of a telescope and an aspherical lens that focuses radiation onto a digital matrix.

To obtain an image of atoms in a dipole trap, the recording of photons associated with fluorescence induced by radiation from cooling lasers is used. The scattering rate Γ_{sc} of photons is determined by the natural transition width Γ, the ratio $S = I/I_s$ of the laser radiation intensity to the saturation intensity, and the laser radiation frequency detuning Δ from resonance [21]:

$$\Gamma_{sc} = \frac{\Gamma}{2} \frac{I/I_s}{1 + I/I_s + 4(\Delta/\Gamma)^2}. \quad (3)$$

In our experiments, the typical saturation parameter value $S \approx 15$ (in experiments with the ^{87}Rb isotope), and $S \approx 20$ (in experiments with the ^{85}Rb isotope). At frequency detuning $\Delta = 2\Gamma$ and $S \approx 15$, a single atom scatters $\sim 9 \times 10^6$ photon s^{-1}. With no allowance for optical system losses, the fraction of photons collected by objective lens is determined by the $NA^2/4$ value and does not exceed 0.7%, which gives a flux of $\sim 7 \times 10^4$ photon s^{-1}.

At the same time, the light shifts induced by the dipole trap's laser radiation remove the atom from resonance with the radiation of cooling lasers. To compensate for these light shifts, we used the amplitude modulation of the dipole trap's laser radiation by a meander in the frequency range of 250 kHz–1 MHz. To avoid parametric heating of atoms in the dipole trap, the amplitude modulation frequency must substantially exceed the doubled resonant frequency of atomic vibrations in the dipole trap [1], which, according to calculations, in our experiments does not exceed 50 kHz. In addition, the turn-off time of the dipole trap laser should be small enough so that the atoms do not have time to leave the trap. In our experiments, the maximum laser turn-off time should not have exceeded 2 μs. The probability of the loss of atoms in an optical dipole trap decreases with increasing modulation frequency. At the same time, the maximum amplitude modulation frequency is limited by the duration of the laser pulse front formed by the acousto-optic modulator (the typical value in our experiments is 100 ns). In the regime of amplitude modulation at a large optical potential depth, atoms effectively interact with resonant laser radiation only when the dipole trap laser is turned off. This reduces the effective exposure time by half when modulating by meander. The selection of the modulation signal's duty cycle within small limits can be used to optimise the parameters of capture and observation of single atoms [9].

The time diagram of the experiment is shown in Fig. 4. Rubidium atoms are loaded into the dipole trap from a magneto-optical trap for 100 ms–1 s (depending on the density of atoms in the vacuum chamber). Then the magnetic field gradient, cooling laser, and repump laser are turned off. Within 100 ms, atoms leave the magneto-optical trap, which is necessary to eliminate background signals from atoms that are not trapped into the dipole trap. After that, to detect atoms in the dipole trap, the cooling and repump lasers are turned on for a time of 30–200 ms. Simultaneously, the amplitude modulation of the dipole trap laser is turned on to reduce the effect of light shifts on the intensity of resonance fluorescence. The video camera exposure is monitored by an external trigger via the CameraLink interface. After the initial recording of atoms, all lasers are turned off for a given time of 50 ms–2 s, except for the dipole trap laser.

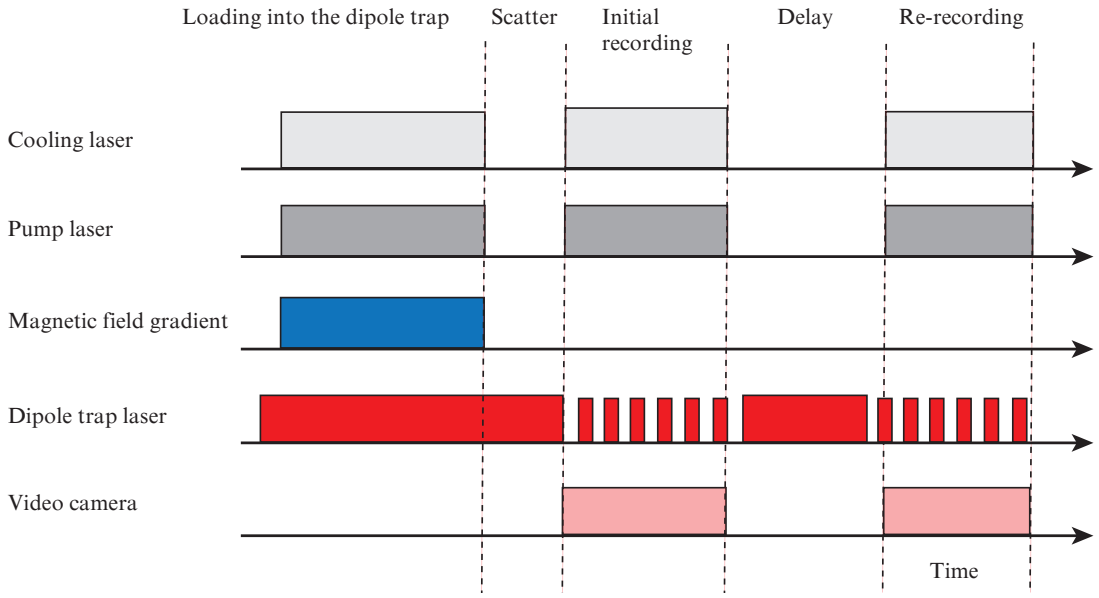

Figure 4. Time diagram of the experiment on trapping and recording of rubidium atoms in an optical dipole trap.

Then the atoms in the dipole trap are re-recorded, which allows us to estimate the loss of single atoms between frames. At the experimental cycle's end, the magnetic field gradient is turned on again, and the reloading of atoms into the magneto-optical and dipole traps starts.

Figure 5 shows images obtained using a digital video camera, which correspond to the absence of atoms in the dipole trap (Fig. 5a), trapping of a single atom (Fig. 5b), and trapping of two atoms (Fig. 5c). Figure 5d shows successively measured radiation intensities of atoms in a dipole trap after subtracting the illumination level averaged over four pixels. The exposure time was 200 ms. Signal levels corresponding to noise signals, and also to trapping of a single atom and two atoms into a dipole trap are clearly distinguishable. This allowed us to systemise images, examples of which are shown in Figs 5a–5c, and determine the number of atoms recorded in each image.

It should be noted that the image size of the fluorescing atom in Fig. 5b corresponds to the image size of the optical fibre's end-face in Fig. 3a. At the same time, the mode field diameter for this optical fibre is 5.3 μm, which is significantly less than the focused laser beam diameter (according to the data in Fig. 2). This indicates a better localisation of atoms in the dipole trap within a region, the diameter of which does not exceed 6 μm.

We also conducted an experiment to record single ^{87}Rb atoms in continuous regime. The cooling and repump lasers remained switched on continuously. Frequency detuning of cooling laser radiation from the resonance with the transition frequency of $5S_{1/2}(F = 2) \rightarrow 5P_{3/2}(F = 3)$ to the red side in ^{87}Rb was 19.4 MHz. The dipole trap's laser radiation was modulated in amplitude by a meander at a frequency of 1 MHz to reduce the effect of light shifts on the fluorescence signal intensity. To reach the single-atom regime, the rate of loading atoms into the magneto-optical trap was selected by changing the current passing through the dispensers that served as a source of rubidium atoms. Images of atoms were continuously recorded by the Flir Tau CNV video camera at a frequency of 5 frames per second (exposure time 199 ms). The time dependence of the optical dipole trap's signal intensity is shown in Fig. 6. This dependence has a form of the well-known 'telegraph' signal [1]: in the absence of atoms in the optical dipole trap, a near-zero noise signal is recorded, whereas, when the atom is trapped, an almost constant average signal level is recorded, which decreases to zero when the atom leaves the dipole trap. In our experiments, the maximum observation time for single atoms was about 40 s.

4. Analysis of statistics on recording atoms in a dipole trap

For a more detailed analysis of the statistics on detecting single atoms, histograms of the radiation intensity distribution of atoms in a dipole trap were constructed after subtracting the average noise level for an exposure time of 30, 50, 100, and 200 ms (Fig. 7). Each histogram was plotted according to the

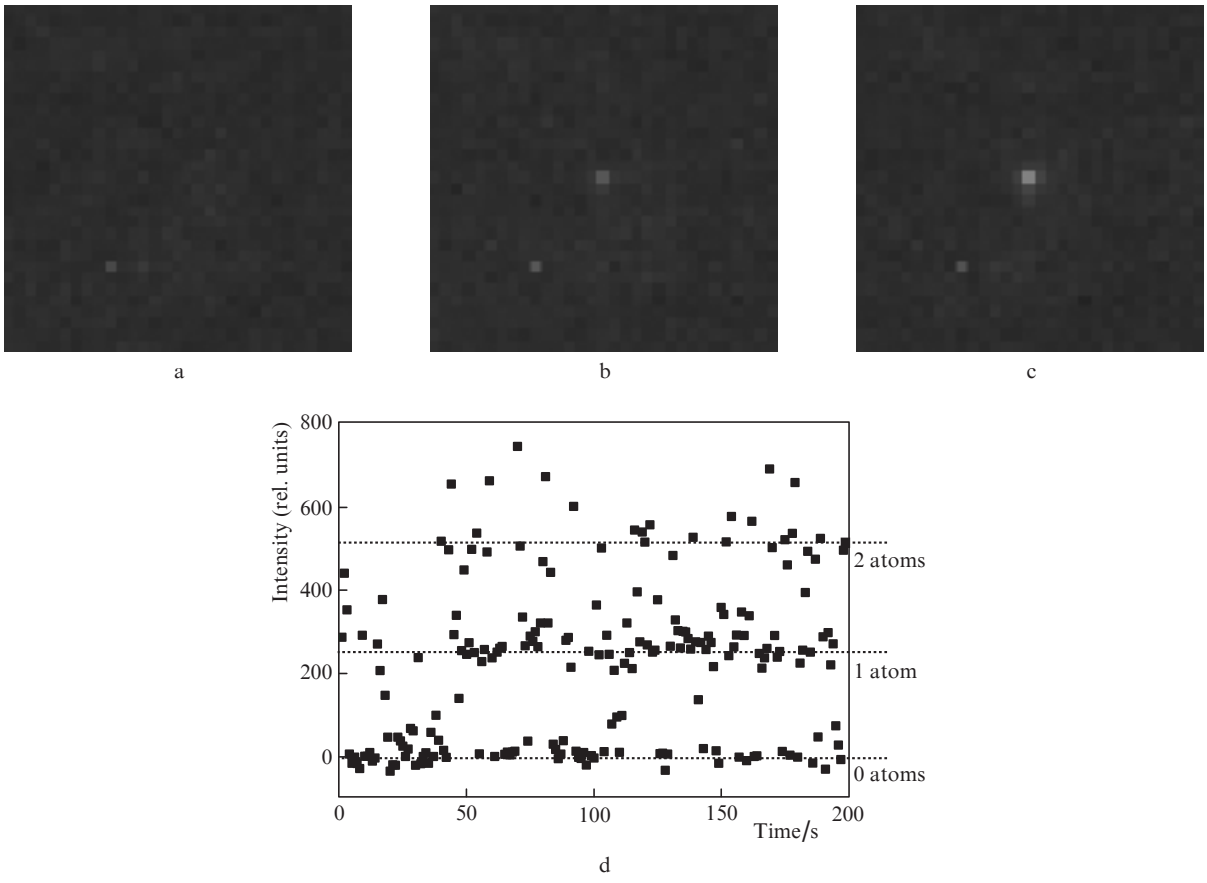

Figure 5. Images obtained by a video camera: (a) in the absence of atoms in the dipole trap, (b) trapping of a single atom, and (c) trapping of two atoms; (d) recorded radiation intensity of atoms in the dipole trap for 200 consecutive measurements with an interval of 1 s.

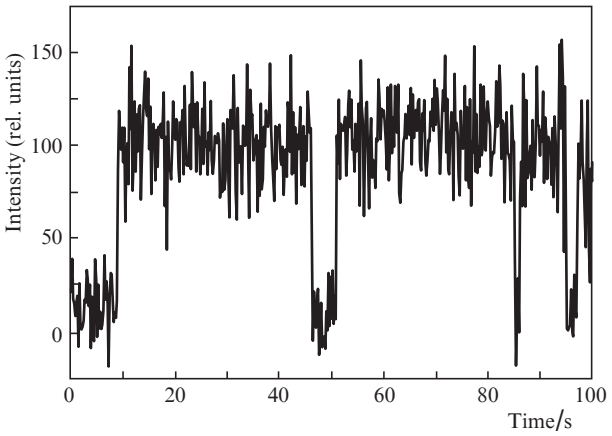

Figure 6. Time dependence of the fluorescence signal intensity of atoms in an optical dipole trap.

results of 200 consecutive measurements (initial recording in Fig. 4). It can be seen that the intensity distribution has a form of discrete peaks.

Loading atoms into a dipole trap is stochastic. Since the number of photons emitted by each atom in the dipole trap during the observation time is much greater than unity, the fluorescence intensity distribution for each peak has a form of the Gaussian function

$$G_i(x) = \frac{A_i}{\sigma_i\sqrt{2\pi}}\exp\left[-\frac{(x-a_i)^2}{2\sigma_i^2}\right], \quad (4)$$

where A_i is the area under the plot; a_i is the profile centre; and σ_i is the standard deviation. The resolution by the number of atoms is attained when the intensity distribution histogram consists of clearly distinguishable peaks corresponding to the signal noise level, the fluorescence of a single atom, and also the fluorescence of two atoms in cases when the probability of their simultaneous loading into the dipole trap cannot be ignored (Figs 7b–7d). Then it is possible to establish a threshold signal level value that separates the monatomic signal from the noise or diatomic signals. For example, in Fig. 7d, thresholds for a single-atom signal are taken at the intensity level of 150 and 400 relative units (photocounts).

If two adjacent Gaussian peaks are noticeably overlapped, the measurement result associated with their overlap area cannot be unambiguously attributed to one or the other peak. This allows us to estimate the error in determining the number of atoms by approximating the experimental data with Gaussian functions. As a measure of error, we have introduced the ratio of the sum S_{01} of the overlap integrals for the monoatomic and noise peaks, as well as that of the corresponding sum S_{12} for the monoatomic and diatomic peaks, to the area S_1 of the peak related to the single-atom signal:

$$Q = \frac{S_{01} + S_{12}}{S_1}. \quad (5)$$

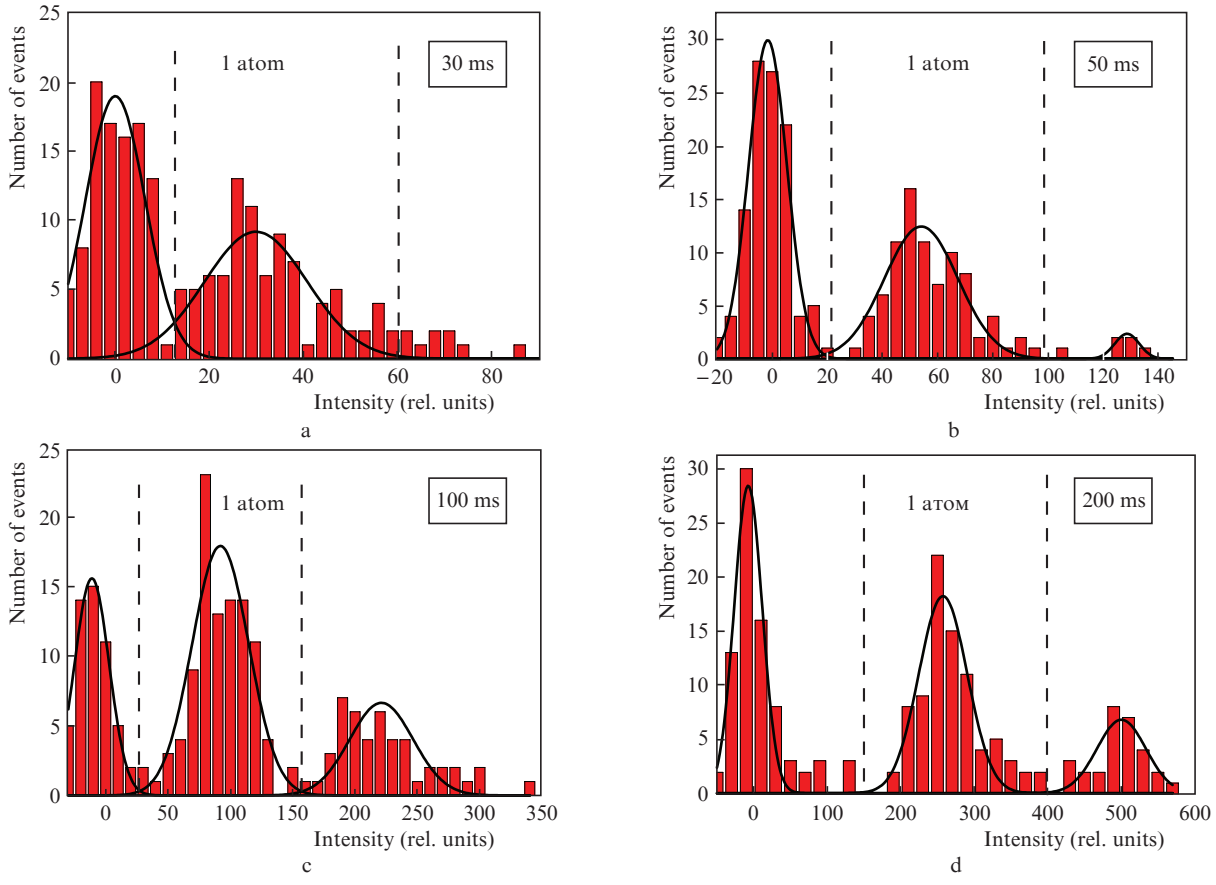

Figure 7. Radiation intensity distributions of atoms in a dipole trap after subtracting the average noise level for exposure times of (a) 30, (b) 50, (c) 100, and (d) 200 ms.

The overlap region of two Gaussian peaks is schematically shown in Fig. 8. For two Gaussian functions described by the parameters $A_{1,2}$, $a_{1,2}$, and $\sigma_{1,2}$, the coordinate of their intersection point in the case when $a_1 < a_2$ and $\sigma_1 \neq \sigma_2$ is given by the expression

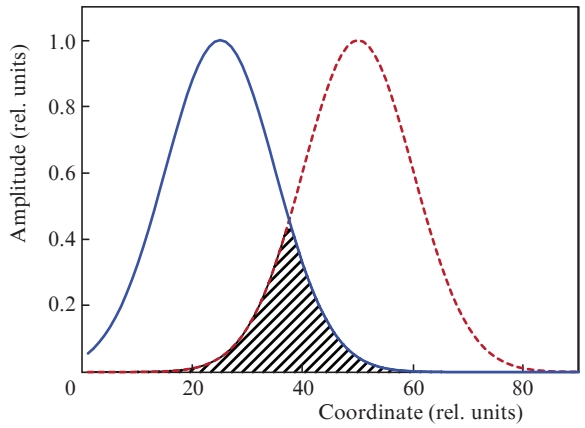

Figure 8. Overlap area of two Gaussian functions.

$$c_{12} = \frac{a_2\sigma_1^2 - a_1\sigma_2^2}{\sigma_1^2 - \sigma_2^2} - \frac{\sqrt{\sigma_1^2\sigma_2^2\{(a_1 - a_2)^2 - 2(\sigma_1^2 - \sigma_2^2)\ln[A_1\sigma_2/(A_2\sigma_1)]\}}}{\sigma_1^2 - \sigma_2^2}. \quad (6)$$

In the trivial case of $\sigma_1 = \sigma_2$, we have $c_{12} = (a_2 + a_1)/2$. The overlap area integral is expressed through the error function:

$$S_{12} = \frac{A_1}{2}\left[1 + \mathrm{erf}\left(\frac{c_{12} - a_1}{\sigma_1\sqrt{2}}\right)\right] + \frac{A_2}{2}\left[1 + \mathrm{erf}\left(\frac{c_{12} - a_2}{\sigma_2\sqrt{2}}\right)\right]. \quad (7)$$

For exposure times of 50 and 100 ms, our error estimate does not exceed 2.5%. At an exposure time of 30 ms, the error in determining the number of atoms exceeds 12%. Thus, effective observation of single atoms in our experiment is possible for an exposure time of 50 ms, which is also typical for experiments using more advanced EMCCD cameras.

To estimate the loss of atoms in the dipole trap, the measured histograms were used to determine the threshold signal levels corresponding to the recording of a single atom at each exposure time value. After that, the single-atom records obtained during the initial recording stage were selected. Then, records were selected from them, in which the atom also remained during the secondary recording with a delay of 200 ms between frames. This made it possible to determine the probability of re-recording of a single atom. The dependence of the measured probability on time is shown in Fig. 9. In our experiments, the maximum probability of re-recording single atoms does not exceed 90%, which may be due to their collisions with hot atoms from the atomic beam source. However, as the exposure increases, there is no significant reduction in the probability of re-recording, despite the overall increase in the observation time for obtaining two images.

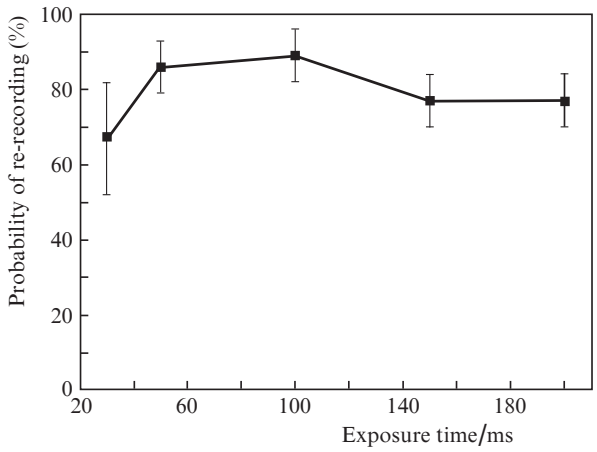

Figure 9. Dependence of the re-recording probability of atoms in a dipole trap on the exposure time.

This indicates that even with long-term observation of atoms in the conditions of their interaction with the radiation of cooling lasers and amplitude modulation of the laser radiation of a dipole trap, significant heating of the atoms did not occur. On the contrary, detection of atoms using cooling lasers may lead to a decrease in their temperature [9].

5. Conclusions

In this work, we demonstrated the trapping of single rubidium atoms in an optical dipole trap using a long-focus objective lens with a relatively small numerical aperture (NA = 0.172) and a sCMOS video camera for detecting trapped atoms by the resonance fluorescence method. We estimated the error in measuring the number of trapped atoms and measured the probability of re-recording of single atoms as a function of exposure time.

Although highly sensitive EMCCD cameras and photon counters are widely used for experiments with single atoms, the parameters of modern sCMOS cameras are sufficient for successful experiments with single atoms and large atomic arrays due to the low level of dark noise. This makes it possible to use them even in experiments where the efficiency of photon collection is limited by small numerical aperture of the optics used. At the same time, unlike photon counters, sCMOS cameras have a spatial resolution that allows experiments with arrays of atoms.

Acknowledgements. The authors are grateful to Mark Saffman, Peng Xu, S.S. Straupe, S. Bergamini, P.L. Chapovsky, and J.D. Pritchard for valuable discussions.

This work was supported by the Foundation for Advanced Research in part of trapping single atoms in an optical dipole trap, their recording, and estimating the error in measuring the number of captured atoms. The work on measuring the dependence of the re-recording probability on the exposure time was supported by the Russian Science Foundation (Project No. 18-12-00313), as well as by Novosibirsk State University and the Russian Academy of Sciences.

References

1. Schlosser N., Reymond G., Protsenko I., Grangier P. *Nature*, **411**, 1024 (2001).

2. Schlosser N., Reymond G., Grangier P. *Phys. Rev. Lett*., **89**, 023005 (2002).
3. Weber M., Volz J., Saucke K., Kurtsiefer C., Weinfurter H. *Phys. Rev. A*, **73**, 043406 (2006).
4. Sortais Y.R.P., Marion H., Tuchendler C., Lance A.M., Lamare M., Fournet P., Armellin C., Mercier R., Messin G., Browaeys A., Grangier P. *Phys. Rev. A*, **75**, 013406 (2007).
5. Zuo Z., Fukusen M., Tamaki Y., Watanabe T., Nakagawa Y., Nakagawa K. *Opt. Express*, **17**, 22898 (2009).
6. Xu P., He X., Wang J., Zhan M. *Opt. Lett*., **35**, 2164 (2010).
7. Li X., Zhou F., Ke M., Xu P., He X., Wang J., Zhan M. *Appl. Opt*., **57**, 7584 (2018).
8. Pritchard J.D., Isaacs J.A., Saffman M. *Rev. Sci. Instr*., **87**, 073107 (2016).
9. Picken C.J., Legaie R., Pritchard J.D. *Appl. Phys. Lett*., **111**, 164102 (2017).
10. Urban E., Johnson T.A., Henage T., Isenhower L., Yavuz D.D., Walker T.G., Saffman M. *Nature Phys*., **5**, 110 (2009).
11. Bochmann J., Mücke M., Guhl C., Ritter S., Rempe G., Moehring D.L. *Phys. Rev. Lett*., **104**, 203601 (2010).
12. Bergamini S., Darquié B., Jones M., Jacubowiez L., Browaeys A., Grangier P. *J. Opt. Soc. Am. B*, **21**, 1889 (2004).
13. Nogrette F., Labuhn H., Ravets S., Barredo D., Béguin L., Vernier A., Lahaye T., Browaeys A. *Phys. Rev. X*, **4**, 021034 (2014).
14. Barredo D., de Léséleuc S., Lienhard V., Lahaye T., Browaeys A., *Science*, **354**, 1021 (2016).
15. Barredo D., Lienhard V., Léséleuc S. de, Lahaye T., Browaeys A., *Nature*, **561**, 79 (2018).
16. Samoylenko S., Lisitsin A., Schepanovich D., Bobrov I., Straupe S., Kulik S. arXiv:2001.02979 (2020).
17. Piotrowicz M.J., Lichtman M., Maller K., Li G., Zhang S., Isenhower L., Saffman M. *Phys. Rev. A*, **88**, 013420 (2013).
18. Graham T.M., Kwon M., Grinkemeyer B., Marra Z., Jiang X., Lichtman M.T., Sun Y., Ebert M., Saffman M. *Phys. Rev. Lett*., **123**, 230501 (2019).
19. Levine H., Keesling A., Semeghini G., Omran A., Wang T.T., Ebadi S., Bernien H., Greiner M., Vuletić V., Pichler H., Lukin M.D. *Phys. Rev. Lett*., **123**, 170503 (2019).
20. Lee W., Kim M., Jo H., Song Y., Ahn J. *Phys. Rev. A*, **99**, 043404 (2019).
21. Grimm R., Weidemüller M., Ovchinnikov Y.B. *Opt. Phys*., **42**, 95 (2000).
22. McGuirk J.M., Harber D.M., Obrecht J.M., Cornell E.A. *Phys. Rev. A*, **69**, 062905 (2004).
23. Abel R.P., Carr C., Krohn U., Adams C.S. *Phys. Rev. A*, **84**, 023408 (2011).
24. https://andor.oxinst.com/.
25. Communal J. *6th Workshop on Hyperspectral Image and Signal Processing: Evolution in Remote Sensing (WHISPERS)* (Lausanne, 2014) pp 1–4.